J Mol Model (2013) 19:5237–5244
DOI 10.1007/s00894-013-2019-1

ORIGINAL PAPER

Coupling of mechanical and electronic properties of carbon nanotubes

Dahiyana Cristancho · Laura Benitez · Jorge M. Seminario

Received: 19 August 2013 / Accepted: 22 September 2013 / Published online: 15 October 2013

Abstract Because of the potential importance of carbon nanotubes (CNT) in renewable energy and other fields, molecular orbital ab initio calculations are used to study the relation between mechanical and electronic properties of such structures. We estimate a modulus of elasticity of 1.3 TPa and find out that the mechanism of CNT structure deformation is dependent on their chirality. Armchair and chiral nanotubes have ductile deformation fracture while zigzag have both ductile and brittle; on the other hand armchair nanotubes fracture and form two caps while chiral nanotubes adopt a helical-structure conformation. In addition, the energy gap between occupied and unoccupied molecular orbitals increases when nanotubes are under plastic deformation. This strong coupling between mechanical and electrical properties can be used to tune CNT mechanically to specific electronic bandgaps, affecting directly their electromagnetic absorption properties.

Keywords Carbon nanotubes · Coupling · Gap · Mechanical–electrical · Molecular Orbitals · Strain · Stress

Introduction

Despite the great technological development in the past years, experimental characterization of mechanical properties at the nanoscale is still challenging because of the small size of the structures, which makes manipulation, observation, and measurement of applied forces not very accurate [1]. Hence, quantum mechanical techniques offer the advantage of calculating in a very precise way, the physical-chemical properties of molecular systems and provide a good estimation of the molecular structure, orbitals, and defects of a material under external forces; most of these properties are difficult to observe experimentally. Molecular modeling is also important to get initial or guess parameters for the design of new nanomaterials and nanodevices. A new nanomaterial in a mechanical assembly is subject to external forces that stretch, deform and, if the applied loads are in excess, destroy the material. Thus, it is important to know whether the material will be strong enough to resist the loads that it will suffer during service. For this reason, scientists have focused on the search and design of tensile tests using several methodologies and approaches to characterize the MPs of nanostructures such as carbon nanotubes (CNT). Carbon nanotubes are cylindrical nanostructures of carbon atoms forming hexagonal rings (Fig. 1) and they are generally illustrated as the rolling up of graphene (one-carbon atom thick sheets); according to how this material is wrapped, they are classified as armchair, zigzag, and chiral (Fig. 1a–e).

Properties such as the modulus of elasticity (*E*) of CNT have been reported using experimental techniques and theoretical approaches (Table 1). Experimentally, mechanical properties of CNTs have been studied primarily using two microscopy techniques: the transmission electron microscopy [2], and the atomic force microscopy [3]. Treacy et al. [4] found, for the first time, a value of 1.8 TPa for the elastic modulus of CNT using transmission microscopy by observing the thermal vibrations, and *E* was estimated from the frequencies of the first two resonant modes [5]. In 2007, Wong et al. [2] found a value of 1.28 TPa by using AFM to bend multiwall carbon nanotubes, and then measured their deflection as a

D. Cristancho · L. Benitez · J. M. Seminario (✉)
Department of Chemical Engineering, Texas A&M University, College Station, TX, USA
e-mail: seminario@tamu.edu

D. Cristancho · J. M. Seminario
Department of Materials Science and Engineering, Texas A&M University, College Station, TX, USA

L. Benitez · J. M. Seminario
Department of Electrical and Computer Engineering, Texas A&M University, College Station, TX, USA

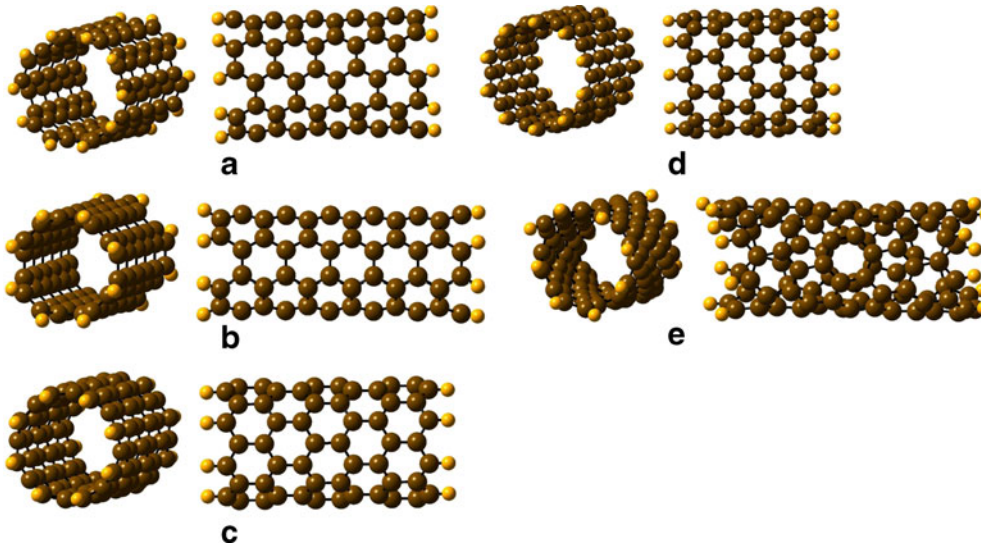

Fig. 1 Longitudinal (left) and side (right) views of optimized carbon nanotube structures used in the current study. (**a**) CNT(5,5) (**b**) CNT(4,4) (**c**) CNT(8,0) (**d**) CNT(10,0) and CNT(6,2). C: brown, H: yellow

function of the applied force and as a function of the displacement from its equilibrium [2]; E was extracted from the slope of the deflection versus force curve [3]. Nonetheless, using atomic force microscopy or transmission electron microscopy might hamper observing the details of the atomic structures, deformations, dislocations, crack propagations, and faults at every point of the stress–strain curve. The identification of these defects allows further explanation of the changes in the materials properties of CNTs and plays an important role in processes such as deformation, annealing, diffusion [6], widening in this way the number of CNT applications.

Material and thermal properties of CNTs are attributed to their unique structure of covalent (shared) bonding of sp^2 hybridized carbon atoms forming strong σ and π bonds between carbon atoms [21]. CNT average elastic modulus of ~1.18 TPa and thermal conductivity [22] of 3500 Wm^{-1} K^{-1} are comparable to those of diamond, 1.22 TPa and 3,320 Wm^{-1} K^{-1}, [23] respectively. On the other hand, Politzer et al. [24] found that end-substituted zig-zag nanotubes show a marked gradation of charge along their axes, which could be of extreme interest to tune their mechanical properties. Later on, Xiao et al. [25] found that tuning a donor orientation, relative to the CNT, can significantly enhance the first hyperpolarizability. CNTs are commonly used in composites [26] to reinforce materials such as polymers [27], ceramics, and metals [28].

A deep understanding of the relation between mechanical and electronic properties is important to expand the implementation of CNTs in practical applications; for example, in energy storage devices, Ren et al. [29] studied twisted multi-

Table 1 Estimations of the modulus of elasticity (E) using several approaches. Data from Krishnan et al. [7], Van Lier et al. [8] Li and Chou [9] Natsuki et al. [10] Pantano et al. [11] Gupta et al. [12] and Wu et al. [13] is taken from Khoury et al. [14]. Finite element methods (FEM), high-resolution transmission electron microscopy (HRTEM)

Year	Authors	Method	E (TPa)
1996	Treacy et al. [4]	Transmission electron microscopy	1.8
1997	Wong et al. [2]	Atomic force microscopy	1.28
1998	Krishnan et al. [7]	Thermal vibrations	1.30
2000	Van Lier et al. [8]	Ab initio	1.14
2003	Li and Chou [9]	Structural Mechanics	1.04
2004	Mylvaganam et al. [15]	Molecular dynamics	4.88
2004	Natsuki et al. [10]	Molecular structural mechanics	1.10
2004	Pantano et al. [11]	Continuum shell modeling	4.75
2005	Gupta et al. [12]	Hydrostatic pressure	1.22
2006	Wu et al. [13]	Molecular mechanics	1.06
2008	Wu et al. [16]	STM and magnetic actuation	0.97
2009	Rossie et al. [17]	Molecular Mechanics	0.92
2010	Shokrieh et al. [18]	Nanoscale Continuum Mechanics	1.04
2011	Arenal et al. [19]	HRTEM/AFM	1.11
2012	Rafiee and Heidarhaei [20]	Non Linear FEM	1.33

walled CNTs/MnO_2 and found that this composite can be employed as electrode to create both supercapacitors and lithium-ion microbatteries, and thus introduced carbon nanotubes in the field of conventional energy storage systems. Among CNTs current applications are graphene nanoribbons [30], drug delivery systems [31, 32], tips for atomic force microscopy [33], scaffolds for bone growth [34], synthetic muscles [35], composites [36], coatings [37], solar cells [38], lasers [39], concretes [40], potent strength fibers [41], and fire prevention [42].

Recently, we studied the functionalization of carbon nanotubes with poly(ethylene glycol) for drug delivery applications [43], the design of self-assembled DNA-CNT [44], the interactions of DNA and CNTs [45–47], and also the mechanism of the unzipping of CNTs using potassium permanganate for the potential fabrication of graphene nanoribbons [48]. Here, we extend our understanding of CNTs, by calculating and studying the relationship between their mechanical and electronic properties. Although, the measurement of the mechanical properties of carbon nanotubes has been the focus of several research studies, there is still a controversy or doubts on whether carbon nanotubes are the stiffest materials known so far. In this study, we calculate the elastic modulus of CNTs, determine their stress versus strain curve, analyze their deformation structure until fracture, and finally correlate their mechanical properties with electronic properties, using ab initio quantum chemistry calculations.

Methodology

In this work, CNT(n,n), n=4, 5; CNT(n,0), n=8, 10; and CNT(6,2) are analyzed to calculate their modulus of elasticity; they are passivated with hydrogen atoms at their dangling ends to transform the edge carbon atoms into coordination three sites, and to avoid reconstruction of the atomic structure after optimization (Fig. 1). First, all the initial geometries are optimized to a local minimum using the unrestricted B3PW91/6-31G(*d*) level of theory [49] as coded in the program Gaussian 09 [50]. The hybrid functional B3PW91 has been tested in several applications involving transition metals [51–54], graphene systems [55, 56], and transport properties [57–59], among others. Local minima are tested by performing second derivative calculations only for optimized geometries under zero strain. As an initial guess, the highest occupied molecular orbital (HOMO) and the lowest occupied molecular orbital (LUMO) are mixed to break the α and β spatial symmetries. Then, each carbon nanotube is strained and reoptimized by keeping the hydrogen and carbon atoms located at the ends fixed at their strained locations. At every applied strain, the inner atoms adopt their most stable conformation after each optimization. This procedure is repeated until the CNTs fracture.

For a CNT of radius r and length L, the modulus of elasticity ($E=\sigma/\varepsilon$) is calculated as the slope in the linear region of the stress (σ) versus strain ($\varepsilon=\Delta L/L$) curve. The stress σ (F/A) is the applied force (F) per cross section area ($A=\pi r^2$) of the CNT and ΔL is the change of length of the CNT when the force (F) is applied along its axis. If the total energy of the CNT is W, then $F=-\mathrm{d}W/\mathrm{d}L$. In this work, the yield strength (f_y) is calculated using an offset of 0.002, the tensile strength (f_T) is calculated as the maximum of the stress–strain curve, the fracture point (f_F) is computed as the last point in the stress–strain curve (f_F, ε_F), and the toughness (Ω) as

$$\Omega = \int_0^{\varepsilon F} \sigma d\varepsilon$$

Results and discussion

Mechanical properties

Figure 2 shows the stress–strain curve of CNT(n,n), n=4, 5; CNT(m,0), m=8, 10; and CNT(6,2). Three behaviors can be identified in the curve: elastic, plastic, and fracture. Stress is directly proportional to strain in the elastic region with an average elasticity modulus of 1.31 TPa (Fig. 2) in good agreement with those reported in the literature (Table 1). CNT(8,0) is the stiffest and CNT(5,5) is the most flexible with E of 1.91 and 0.94 TPa, respectively (Table 2). This difference is because in the zigzag the stretching affects mainly an angular bending but a bond stretching in the armchair; this later bond eventually breaks (Fig. 3). In addition, both ductile and brittle behaviors are observed in the stress–strain curve; CNT(4,4), CNT(5,5), CNT(8,0), and CNT(6,2) behave as ductile materials with plastic deformation whereas CNT(10, 0), which is fractured while it is deformed elastically, behaves as a brittle material. These behaviors were also observed by Coluci et al. [60] who also studied the mechanical properties

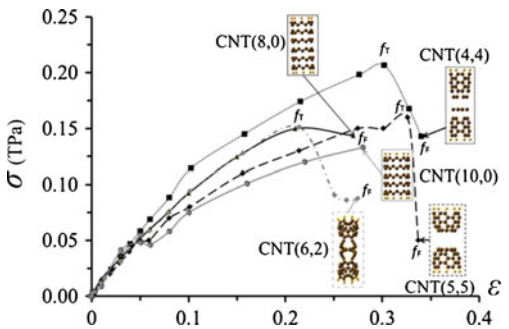

Fig. 2 Tensile strength (f_T), fracture (f_F) and stress (σ) versus strain (ε) points for CNT(n,n) with n=4, 5; CNT(m,0) with m=8, 10; and CNT(6, 2). The calculated E are 1.20, 0.94, 1.91, 1.450 and 1.01 TPa, respectively. All structures are optimized geometries at the fracture points

Table 2 Young modulus (E), yield strength (f_y), tensile strength (f_T), fracture (f_F), and toughness (Ω) of CNTs. All mechanical properties are in TPa except for Ω which is J/m^3

CNT	C_nH_n	Point group	E	f_y	f_T	f_F	Ω ($\times 10^{10}$)
(4,4)	$C_{95}H_{16}$	D_{4d}	1.20	0.07	0.19	0.13	4.32
(5,5)	$C_{100}H_{20}$	D_{5d}	0.94	0.04	0.02	0.06	3.56
(8,0)	$C_{96}H_{16}$	C_1	1.91	0.02	0.15	0.14	2.78
(10,0)	$C_{100}H_{20}$	C_{2V}	1.50	0.05	0.13	0.13	2.37
(6,2)	$C_{100}H_{16}$	D_2	1.01	0.06	0.15	0.28	2.48

of carbon nanotubes and found that zigzag and armchair nanotubes behave as brittle and ductile materials, respectively. In all of the CNTs structures examined in the current study, except CNT(10,0), the stress increases to a maximum stress (f_T) and then decreases to the final fracture (f_F). CNT(10,0) stress increases and stops at the maximum point f_T of 0.13 TPa which is equal to f_F. However, CNT(4,4), CNT(5,5), CNT(6, 2), and CNT(8,0) experience plastic deformation because they have a maximum value of f_T that differs from its fracture value, f_F (Tables 2).

The fracture of nanotubes goes through three well-defined steps: flaw formation, flaw propagation, and rupture. However, every nanotube structure undergoes different fracture pathways, which are chirality dependent (Fig. 2). We re-optimized the geometries of CNTs at every point of the stress–strain curve. We find that armchair nanotubes deform and fracture plastically; once the external stress goes beyond f_T, the nanotubes experience *necking*, which is confirmed by a decrease in the diameters of CNT(4,4), and CNT(5,5) from 0.553 to 0.407 nm and from 0.881 to 0.462 nm, respectively. Two structures are found for CNT(5,5) at fracture point. The fracture point structure with the lowest energy forms two well-defined caps that can be thought as half-fullerenes (hollow sphere made of carbon atoms) with 16 hexagons, and ten squares. However, the structure with the highest energy breaks into four pieces; two of them are rings of carbon dimers and the other two are conformed of carbon hexagon without deformation in the radial direction. These fracture point structures are created by the reorganization of carbon atoms and the formation of new σ and π-bonds due to the high reactivity of the carbons from the broken bonds, which finally reconstruct to a minimum energy conformation. CNT(4,4), which is the most ductile nanotube with a toughness of 4.32 J/m^3 $\times 10,^{10}$ breaks into four pieces: two rings that are conformed by carbon dimers and two caps of only hexagons (Fig. 2). Carbon dimers are formed when running the CNT(4,4) as a closed shell singlet, which has energy 1084.5 kcal mol^{-1} lower than the corresponding triplet.

On the other hand, fracture of zigzag CNTs takes place without any significant deformation of the structure in the radial direction (Fig. 2); these nanotubes distort only in the direction of the applied stress or axial direction and start cracking in several parts along the axis when they are strained 21 % of their length (Fig. 2).

Chiral fracture occurs in three stages. First, C-C bonds that are located parallel to the direction of the applied stress are broken, increasing their length from 0.142 nm to 2.11 nm, ending in a spiral-shaped conformation which can be thought as the wrapping of two carbon chains. Next, as stretching continues, carbon atoms displace in the direction of the applied stress, and finally, fracture results with the formation of two caps with topological defects (ten hexagons, two pentagons, and two triangles) that are separated by the two carbon chains, in helix conformation and sp^3 hybridization (Fig. 2).

The mechanical properties obtained from the strain–stress curves (Fig. 2) yield higher toughness (3.94×10^{10} J/m^3) for armchair than for zigzag (2.58×10^{10} J/m^3) and chiral (2.48×10^{10} J/m^3) carbon nanotubes (Table 2). This behavior is consistent with the fact that armchair nanotubes are deformed in both, axial (along the applied stress) and radial directions; however, zigzag and chiral are deformed in the axial direction only (Fig. 3). Therefore, nanotubes that are deformed in axial and radial directions absorb higher energy and thus they have better chances for crack propagation and microvoid coalescence (mechanism of fracture in ductile materials). Armchair nanotubes deform and fracture plastically; once the external stress goes beyond f_T, the nanotubes experience *necking*, which is confirmed by a decrease in the diameters of CNT(4,4), and CNT(5,5) from 0.553 to 0.407 nm and from 0.881 to 0.462 nm, respectively, as is shown in the inset Fig. 1.

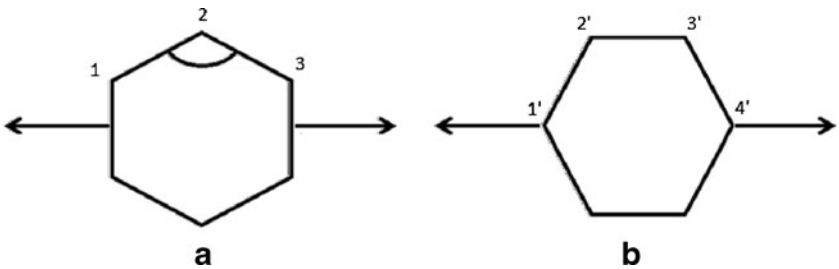

Fig. 3 The direct effect of a longitudinal stress on an (**a**) armchair and (**b**) zigzag CNTs correspond to angular bending and bond stretching, respectively

Electronic properties

To understand the mechanical behavior of carbon nanotubes, frontiers orbitals are calculated using molecular orbital theory. Figure 4 displays the molecular orbital spectra of all nanotubes used in the current study with their corresponding frontier orbital shapes at points from the elastic region, f_y, f_T and f_F. CNT(4,4) HOMO lies at −4.25 eV and has a delocalized orbital that is perpendicular to the stretching direction, while CNT(5,5) HOMO lies at −4.48 eV and has a delocalized orbital along the pulling direction. Delocalization of frontier orbitals is due to the overlapping of the p atomic orbitals that

Table 3 HOMO-LUMO gaps (HLG) of CNTs for the three points of the elastic region (HLG_n with n=0, 1, 2), as well as for the yield strength (HLG_{fy}), tensile strength (HLG_{fT}), and fracture (HLG_F)

CNT	HLG_0	HLG_1	HLG_2	HLG_{fy}	HLG_{fT}	HLG_F
(4,4)	1.26	1.39	1.61	1.14	2.52	2.40
(5,5)	1.70	1.67	–	1.15	2.31	2.30
(8,0)	1.76	1.76	–	1.75	2.01	1.95
(10,0)	1.87	1.87	1.84	0.27	1.73	1.73
(6,2)	1.60	1.60	–	0.28	1.08	1.80

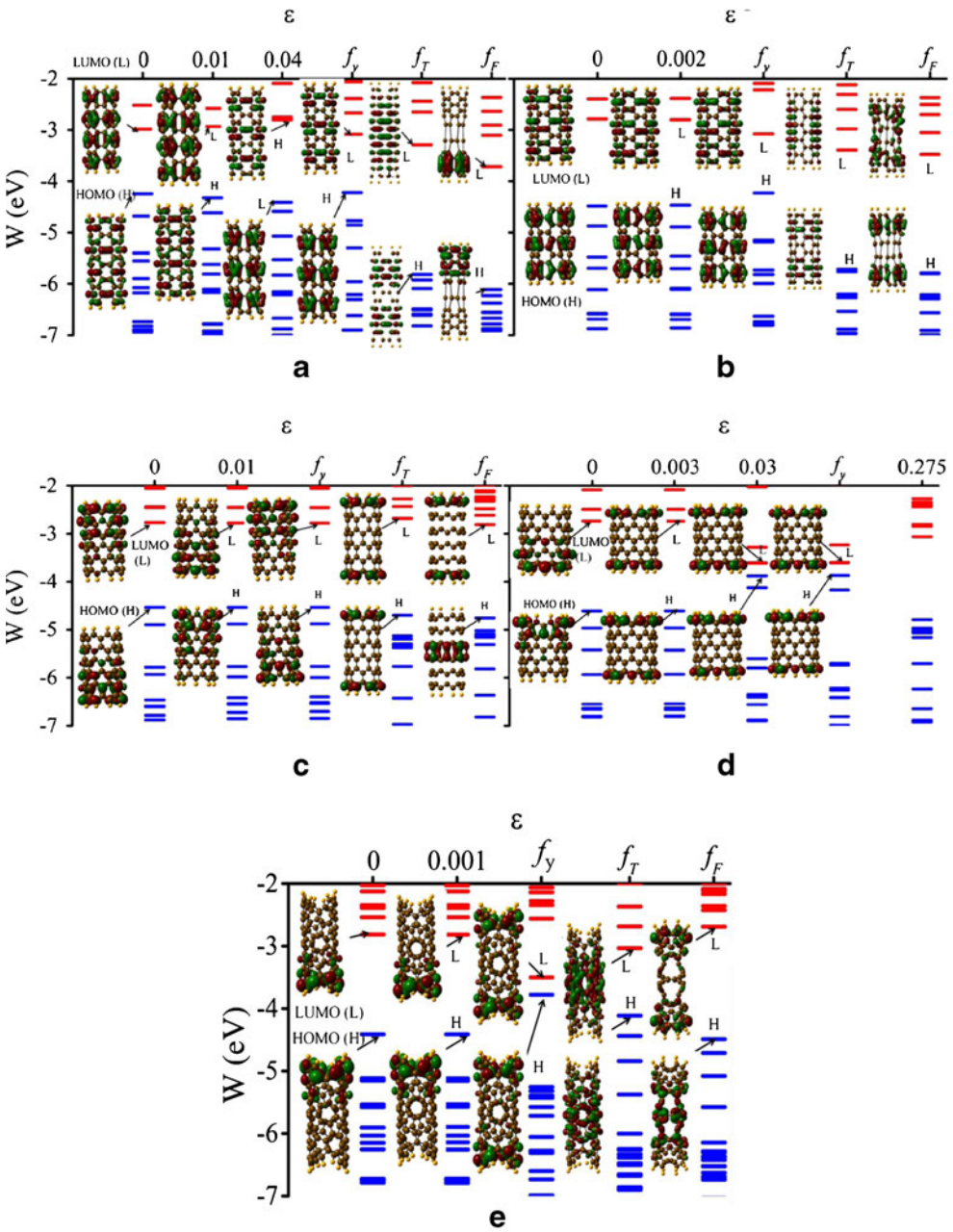

Fig. 4 Occupied (blue) and unoccupied (red) molecular orbital energy spectra at three points from plastic region: f_y, f_T, and f_F. of (**a**) CNT(4,4) including three points from elastic region 0, 0.01, and 0.04, (**b**) CNT(5,5) including two points from elastic region 0 and 0.002 (**c**) CNT(8,0) including two points from elastic region 0 and 0.01 (**d**) CNT(10,0) at three points from elastic region 0, 0.003, and 0.03. (**e**) CNT(6,2) including two points from elastic region 0 and 0.001

do not participate in the bonds. As stretching of CNT(4,4) and CNT(5,5) occurs from 0 to 0.04 and from 0 to 0.002, respectively, their HOMO-LUMO gap increases from 1.26 eV to 1.61 eV and decreases from 1.70 eV to 1.67 eV (Table 3), respectively. Their molecular orbitals stay delocalized on the CNT surface as a consequence of the stability of armchair CNTs under elastic stretching, and the flexibility of the carbon-carbon bonds.

Plastic deformation leads to the breaking of the delocalized orbitals; HOMO and LUMO localize according to the formed carbon-carbon bonds and their HLGs at f_y decrease from 1.26 to 1.14 eV, and from 1.70 to 1.15 eV (Table 3) for CNT(4,4) and CNT(5,5), respectively. At f_T, there is a breaking of the π-bonds of the CNT(n, n); the HOMO is on top of the CNT and then, loss of the π-bonds takes place once the necking starts. At f_T, the HLGs increase up to 2.52 and 2.31 eV (Table 3) for CNT(4,4) and CNT(5,5), respectively. At fracture (f_F), CNT(4,4) HOMO is localized at the bottom of the nanotube while the LUMO is localized at the top of it. The CNT(5,5) HOMO is delocalized in every cap formed at fracture.

On the other hand, zigzag HOMOs are partially delocalized and doubly degenerate. CNT(8,0) HOMO is at the bottom of the nanotube, while CNT(10,0) HOMO is at the upper part. As the nanotube is pulled apart from 0 to 0.01, CNT(8,0) HOMO is located at the upper part of the nanotube, and after f_y, it migrates to the ends of the nanotube (Fig. 4c). Nevertheless, when CNT(10,0) is stretched from 0.003 to f_y, its HOMO does not change its position and it is always kept at the ends of the nanotubes. CNT(8,0) HOMO is localized in the middle part of the nanotube at the fracture point while its LUMO stays at the ends of the nanotube. CNT(6,2) HOMO stays in the upper part and its LUMO in the lower part of the nanotube from 0 to 0.001. However, when it reaches f_y, both HOMO and LUMO split into two parts and then they localize in the middle part of the nanotube at f_T. Finally, at f_F, CNT(6,2) HOMO and LUMO are localized in the two helical carbon chains and caps as is observed in Fig. 4(e).

Consequently, the relation between mechanical and electronic properties reveals that carbon nanotubes that are stretched and deformed up to their tensile strength can be suitable materials for the fabrication of solar cells with absorptions in the range of 1.26–2.52 eV as deduced from the calculated HOMO-LUMO gaps. Also, because of the coupling of mechanical and electrical properties, it may be possible to control the adsorption of solar light from low to high energy by manipulating the stretching of the nanotubes.

Conclusions

Carbon nanotubes have an elastic modulus of 1.3 TPa obtained using ab initio calculations. Armchair and chiral nanotubes have ductile deformation fracture while zigzag ones have both ductile, and brittle. Armchair nanotubes break forming two caps while chiral nanotubes adopt a helical-structure conformation at fracture. HOMO-LUMO energy gaps of all the nanotubes decrease at yield strength and then increase after their tensile strength. Thus, deformed CNT(n,n) with $n=4,5$; CNT(m,0) with $m=8$ and 10; and CNT(6,2) can be suitable materials for the fabrication of solar cells with electromagnetic absorption in the range of 1.26–2.52 eV. The energy gap increase between occupied and unoccupied molecular orbitals when nanotubes are under plastic deformation explains a strong coupling between mechanical and electrical properties that can be used to tune CNT mechanically to specific electronic bandgaps, controlling directly their electromagnetic absorption properties.

Acknowledgments We acknowledge the high-performance computing support provided by the Texas A&M Supercomputer Facility and the Texas Advanced Computing Center as well as the financial support from the U.S. Defense Threat Reduction Agency (DTRA) through the U.S. Army Research Office (ARO), project no. W91NF-06-1-0231; and ARO/MURI project no. W911NF-11-1-0024.

References

1. Minary-Jolandan M., M. Y (2012) Mechanical and electromechanical characterization of one-dimensional piezoelectric nanomaterials. In: Ciofani G, A. M (eds) Piezoelectric nanomaterials for biomedical applications. Nanomedicine and nanotoxicology. Springer Berlin Heidelberg, pp 63–91. doi:10.1007/978-3-642-28044-3_3
2. Wong EW, Sheehan PE, Lieber CM (1997) Nanobeam mechanics: elasticity, strength, and toughness of nanorods and nanotubes. Science 277(5334):1971–1975. doi:10.1126/science.277.5334.1971
3. Yakobson BI, Avouris P (2001) Mechanical properties of carbon nanotubes. Carbon Nanotubes 80:287–327
4. Treacy MMJ, Ebbesen TW, Gibson JM (1996) Exceptionally high Young's modulus observed for individual carbon nanotubes. Nature 381(6584):678–680. doi:10.1038/381678a0
5. Poncharal P, Wang ZL, Ugarte D, de Heer WA (1999) Electrostatic deflections and electromechanical resonances of carbon nanotubes. Science 283(5407):1513–1516. doi:10.1126/science.283.5407.1513
6. Campbell FC (2008) Elements of metallurgy and engineering alloys. ASM International, Materials Park
7. Krishnan A, Dujardin E, Ebbesen TW, Yianilos PN, Treacy MMJ (1998) Young's modulus of single-walled nanotubes. Phys Rev B 58(20):14013–14019. doi:10.1103/PhysRevB.58.14013
8. Van Lier G, Van Alsenoy C, Van Doren V, Geerlings P (2000) Ab initio study of the elastic properties of single-walled carbon nanotubes and graphene. Chem Phys Lett 326(1–2):181–185
9. Lei X, Natsuki T, Shi J, Ni Q-Q (2011) Analysis of carbon nanotubes on the mechanical properties at atomic scale. J Nanomaterials 2011: 1–10. doi:10.1155/2011/805313
10. Natsuki T, Endo M (2005) Structural dependence of nonlinear elastic properties for carbon nanotubes using a continuum analysis. Appl Phys a-Mater Sci Process 80(7):1463–1468
11. Pantano A, Parks DM, Boyce MC (2004) Mechanics of deformation and multi wall carbon nanotubes. J Mech Phys Solids 52(4):789–821
12. Xuemei W, Vijay G, Soumendra NB (2005) Effects of substrate orientation and metal film thickness on the intrinsic strength, intrinsic fracture energy, and total fracture energy of tantalum–sapphire

interfaces. J Am Ceram Soc 88(7):1909–1913. doi:10.1111/j.1551-2916.2005.00422.x
13. Yongdong W, Xiaochun Z, Leung AYT, Weifang Z (2006) An energy-equivalent model on studying the mechanical properties of single-walled carbon nanotubes. Thin-Walled Struct 44(6):667–676
14. Khoury E, Messager T, P. C (2011) Derivation of the Young's and Shear Moduli of single-walled carbon nanotubes through a computational homogenization approach. J Multiscale Comput Eng 9:97–118
15. Mylvaganam K, Zhang LC (2004) Important issues in a molecular dynamics simulation for characterising the mechanical properties of carbon nanotubes. Carbon 42(10):2025–2032. doi:10.1016/j.carbon.2004.04.004
16. Wu Y, Huang M, Wang F, Huang XMH, Rosenblatt S, Huang L, Yan H, O'Brien SP, Hone J, Heinz TF (2008) Determination of the Young's modulus of structurally defined carbon nanotubes. Nano Lett 8(12):4158–4161. doi:10.1021/nl801563q
17. Rossi M, Meo M (2009) On the estimation of mechanical properties of single-walled carbon nanotubes by using a molecular-mechanics based FE approach. Compos Sci Technol 69(9):1394–1398. doi:10.1016/j.compscitech.2008.09.010
18. Shokrieh MM, Rafiee R (2010) Prediction of Young's modulus of graphene sheets and carbon nanotubes using nanoscale continuum mechanics approach. Mater Des 31(2):790–795. doi:10.1016/j.matdes.2009.07.058
19. Arenal R, Wang M-S, Xu Z, Loiseau A, Golberg D (2011) Young modulus, mechanical and electrical properties of isolated individual and bundled single-walled boron nitride nanotubes. Nanotechnology 22 (26). doi:10.1088/0957-4484/22/26/265704
20. Rafiee R, Heidarhaei M (2012) Investigation of chirality and diameter effects on the Young's modulus of carbon nanotubes using nonlinear potentials. Compos Struct 94(8):2460–2464. doi:10.1016/j.compstruct.2012.03.010
21. Dresselhaus MS, Dresselhaus G, Charlier JC, Hernandez E (2004) Electronic, thermal and mechanical properties of carbon nanotubes. Philos Trans R Soc a-Math Phys Eng Sc 362(1823):2065–2098. doi:10.1098/rsta.2004.1430
22. Pop E, Mann D, Wang Q, Goodson KE, Dai HJ (2006) Thermal conductance of an individual single-wall carbon nanotube above room temperature. Nano Lett 6(1):96–100. doi:10.1021/nl052145f
23. Spear K, Dismukes J (1994) Synthetic diamond—Emerging CVD science and technology. Wiley, Chichester, UK
24. Politzer P, Murray J, Lane P, Concha M, Jin P, Peralta-Inga Z (2005) An unusual feature of end-substituted model carbon (6,0) nanotubes. J Mol Model 11(4–5):258–264. doi:10.1007/s00894-005-0265-6
25. Xiao D, Bulat FA, Yang W, Beratan DN (2008) A donor— nanotube paradigm for nonlinear optical materials. Nano Lett 8(9):2814–2818. doi:10.1021/nl801388z
26. Ci L, Suhr J, Pushparaj V, Zhang X, Ajayan PM (2008) Continuous carbon nanotube reinforced composites. Nano Lett 8(9):2762–2766. doi:10.1021/nl8012715
27. Bakshi SR, Lahiri D, Agarwal A (2010) Carbon nanotube reinforced metal matrix composites—a review. Int Mater Rev 55(1):41–64. doi:10.1179/095066009x12572530170543
28. Chen YL, Liu B, Huang Y, Hwang KC (2011) Fracture toughness of carbon nanotube-reinforced metal- and ceramic-matrix composites. JNano Mat. doi:10.1155/2011/746029
29. Ren J, Li L, Chen C, Chen X, Cai Z, Qiu L, Wang Y, Zhu X, Peng H (2013) Twisting carbon nanotube fibers for both wire-shaped micro-supercapacitor and micro-battery. Adv Mater 25(8):1155–1159. doi:10.1002/adma.201203445
30. Rangel N, Sotelo JC, Seminario JM (2009) Mechanism of carbon nanotubes unzipping into graphene ribbons. J Chem Phys 131
31. Bobadilla AD, Samuel ELG, Tour JM, Seminario JM (2013) Calculating the hydrodynamic volume of poly(ethylene oxylated) single-walled carbon nanotubes and hydrophilic carbon clusters. J Phys Chem B 117:343–354
32. Moore TL, Pitzer JE, Podila R, Wang X, Lewis RL, Grimes SW, Wilson JR, Skjervold E, Brown JM, Rao A, Alexis F (2013) Multifunctional polymer-coated carbon nanotubes for safe drug delivery. Part Part Syst Charact 30(4):365–373. doi:10.1002/ppsc.201200145
33. Wilson NR, Macpherson JV (2009) Carbon nanotube tips for atomic force microscopy. Nat Nanotechnol 4(8):483–491. doi:10.1038/nnano.2009.154
34. Zanello LP, Zhao B, Hu H, Haddon RC (2006) Bone cell proliferation on carbon nanotubes. Nano Lett 6(3):562–567. doi:10.1021/nl051861e
35. Aliev AE, Oh J, Kozlov ME, Kuznetsov AA, Fang S, Fonseca AF, Ovalle R, Lima MD, Haque MH, Gartstein YN, Zhang M, Zakhidov AA, Baughman RH (2009) Giant-stroke, superelastic carbon nanotube aerogel muscles. Science 323(5921):1575–1578. doi:10.1126/science.1168312
36. Liao Y, Zhang C, Zhang Y, Strong V, Tang J, Li X-G, Kalantar-zadeh K, Hoek EMV, Wang KL, Kaner RB (2011) Carbon nanotube/polyaniline composite nanofibers: facile synthesis and chemosensors. Nano Lett 11(3):954–959. doi:10.1021/nl103322b
37. Keefer EW, Botterman BR, Romero MI, Rossi AF, Gross GW (2008) Carbon nanotube coating improves neuronal recordings. Nat Nanotechnol 3(7):434–439. doi:10.1038/nnano.2008.174
38. Shi E, Zhang L, Li Z, Li P, Shang Y, Jia Y, Wei J, Wang K, Zhu H, Wu D, Zhang S, Cao A (2012) TiO2-coated carbon nanotube-silicon solar cells with efficiency of 15%. Scientific Reports 2. doi:10.1038/srep00884
39. Baac HW, Ok JG, Maxwell A, Lee K-T, Chen Y-C, Hart AJ, Xu Z, Yoon E, Guo LJ (2012) Carbon-nanotube optoacoustic lens for focused ultrasound generation and high-precision targeted therapy. Scientific Reports 2. doi:10.1038/srep00989
40. Nasibulin AG, Shandakov SD, Nasibulina LI, Cwirzen A, Mudimela PR, Habermehl-Cwirzen K, Grishin DA, Gavrilov YV, Malm JEM, Tapper U, Tian Y, Penttala V, Karppinen MJ, Kauppinen EI (2009) A novel cement-based hybrid material. New Journal of Physics 11. doi:10.1088/1367-2630/11/2/023013
41. Dalton AB, Collins S, Munoz E, Razal JM, Ebron VH, Ferraris JP, Coleman JN, Kim BG, Baughman RH (2003) Super-tough carbon-nanotube fibres - These extraordinary composite fibres can be woven into electronic textiles. Nature 423(6941):703–703. doi:10.1038/423703a
42. Zhao Z, Gou J (2009) Improved fire retardancy of thermoset composites modified with carbon nanofibers. Science and technology of advanced materials 10 (1). doi:10.1088/1468-6996/10/1/015005
43. Bobadilla AD, Samuel ELG, Tour JM, M. SJ (2013) Calculating the hydrodynamic volume of poly(ethylene oxylated) single-walled carbon nanotubes and hydrophilic carbon clusters. J Phys Chem B 117:343–354
44. Bobadilla AD, Seminario JM (2011) DNA-CNT interactions and gating mechanism using MD and DFT. J Phys Chem C 115(8):3466–3474
45. Seminario JM, Agapito LA, Figueroa HP, Ieee I (2002) Towards the design of programmable self-assembled DNA-carbon nanotubes: an approach to nanobiotronics. Proceedings of the 2002 2nd Ieee Conference on Nanotechnology
46. Bobadilla AD, Seminario JM (2012) Self-assembly of a gapped carbon nanotube-DNA molecular junction. J Mol Modeling 18(7):3291–3300
47. Bobadilla AD, Seminario JM (2011) DNA-CNT interactions and gating mechanism using MD and DFT. J Phys Chem C 115(8):3466–3474
48. Rangel NL, Sotelo JC, Seminario JM (2009) Mechanism of carbon nanotubes unzipping into graphene ribbons. Journal of Chemical Physics 131 (3). doi:10.1063/1.3170926
49. Raghavachari K (2000) Perspective on "Density functional thermochemistry. III. The role of exact exchange" - Becke AD (1993) J Chem Phys 98:5648–52. Theoretical Chemistry Accounts 103 (3–4):361–363. doi:10.1007/s002149900065

50. Frisch MJT, G. W.; Schlegel, H. B.; Scuseria, G. E.;, Robb MAC, J. R.; Scalmani, G.; Barone, V.; Mennucci, B.;, Petersson GAN, H.; Caricato, M.; Li, X.; Hratchian, H. P.;, Izmaylov AFB, J.; Zheng, G.; Sonnenberg, J. L.; Hada, M.;, Ehara MT, K.; Fukuda, R.; Hasegawa, J.; Ishida, M.; Nakajima,, T.; Honda YK, O.; Nakai, H.; Vreven, T.; Montgomery, J.; J. A.,, Peralta JEO, F.; Bearpark, M.; Heyd, J. J.; Brothers, E.; Kudin,, K. N.; Staroverov VNK, R.; Normand, J.; Raghavachari, K.;, Rendell AB, J. C.; Iyengar, S. S.; Tomasi, J.; Cossi, M.; Rega,, N.; Millam NJK, M.; Knox, J. E.; Cross, J. B.; Bakken, V.;, Adamo CJ, J.; Gomperts, R.; Stratmann, R. E.; Yazyev, O.;, Austin AJC, R.; Pomelli, C.; Ochterski, J. W.; Martin, R. L.;, Morokuma KZ, V. G.; Voth, G. A.; Salvador, P.; Dannenberg, J. J.; Dapprich, S.; Daniels, A. D.; O. Farkas, Foresman, J. B.; €, Ortiz JVC, J.;, Fox, D. J. Gaussian 09, revision A.02; CT,, W (2009) Gaussian, Inc.
51. Seminario JM, Zacarias AG, Castro M (1997) Systematic study of the lowest energy states of Pd, Pd_2, and Pd_3. Int J Quantum Chem 61: 515–523
52. Seminario JM, Tour JM (1997) Systematic study of the lowest energy states of Au_n (n=1-4) Using DFT. Int J Quantum Chem 65:749–758
53. Seminario JM, Agapito LA, Yan L, Balbuena PB (2005) Density functional theory study of adsorption of OOH on Pt-based bimetallic clusters alloyed with Cr, Co, and Ni. Chem Phys Lett 410(4–6):275–281
54. Balbuena PB, Calvo SR, Lamas EJ, Salazar PF, Seminario JM (2006) Adsorption and dissociation of H_2O_2 on Pt and Pt-alloy clusters and surfaces. J Phys Chem B 110:17452–17459
55. Rangel NL, Seminario JM (2008) Graphene terahertz generators for molecular circuits and sensors. J Phys Chem A 112(51):13699–13705
56. Rangel NL, Sotelo JC, Seminario JM (2009) Mechanism of carbon-nanotubes unzipping into graphene ribbons. J Chem Phys 131(031105):031101–031104
57. Seminario JM, Araujo RA, Yan L (2004) Negative differential resistance in metallic and semiconducting clusters. J Phys Chem B 108(22):6915–6918
58. Derosa PA, Guda S, Seminario JM (2003) A programmable molecular diode driven by charge-induced conformational changes. J Am Chem Soc 125:14240–14241
59. Sotelo JC, Yan L, Wang M, Seminario JM (2007) Field induced conformational changes in bimetallic oligoaniline junctions. Phys Rev A 75 (2):022511-022513
60. Coluci VR, Pugno NM, Dantas SO, Galvao DS, Jorio A (2007) Atomistic simulations of the mechanical properties of 'super' carbon nanotubes. Nanotechnology 18 (33). doi:10.1088/0957-4484/18/33/335702